Journal of Luminescence 208 (2019) 119–124

Contents lists available at ScienceDirect

Journal of Luminescence

journal homepage: www.elsevier.com/locate/jlumin

InGaN/GaN multiple quantum well for superfast scintillation application: Photoluminescence measurements of the picosecond rise time and excitation density effect

Guido Toci[a,b,*], Leonida A. Gizzi[c,d], Petra Koester[c,d], Federica Baffigi[c,d], Lorenzo Fulgentini[c,d], Luca Labate[c,d], Alice Hospodkova[e], Vitezslav Jary[e], Martin Nikl[e], Matteo Vannini[a,b]

[a] Istituto Nazionale di Ottica - Consiglio Nazionale delle Ricerche CNR-INO Sede di Sesto Fiorentino, Via Madonna del Piano 10, Sesto Fiorentino, FI 50019, Italy
[b] Istituto Nazionale di Fisica Nucleare, Sezione di Firenze, Via Giovanni Sansone 1, 50019 Sesto Fiorentino, FI, Italy
[c] Intense Laser Irradiation Laboratory, Istituto Nazionale di Ottica - Consiglio Nazionale delle Ricerche, CNR-INO, Sede di Pisa, Via Moruzzi 1, 56124 Pisa, Italy
[d] Istituto Nazionale di Fisica Nucleare, Sezione di Pisa, Largo Bruno Pontecorvo 3, 56127 Pisa, Italy
[e] Institute of Physics, Academy of Sciences of the Czech Republic, Cukrovarnicka 10, 16200 Prague, Czech Republic

ARTICLE INFO

Keywords:
Multiple quantum wells
InGaN/GaN
Scintillator
Streak camera
Ultrafast rise-time measurements

ABSTRACT

We report the study of the fast rise time and decay time in the ps time scale of the excitonic luminescence of a multiple quantum well (MQW) heterostructure of InGaN/GaN, including the excitation density effect. These structures were proposed as ultrafast scintillators for soft X-ray detectors and particle beam diagnostics. Measurements were carried out with a Hadland Imacon 500 streak camera following excitation of the sample by laser pulses of few tens of μJ at 266 nm and 400 nm, with pulse duration less than 200 fs. The rise time of the detected MWQ luminescence was less than 10 ps, with a possible contribution from the detection system and signal collection geometry. The calibration and the signal processing techniques employed to fully exploit the time resolution of the detection system are also described.

1. Introduction

Inorganic scintillators have many applications in various fields as medical imaging, homeland security, high-tech industry and high energy and nuclear physics [1,2]. In particular, strong interest is motivated by the possibility to achieve a high spatial resolution in positron emission tomography (PET) imaging in medicine [3,4] and in electromagnetic calorimetry which are a part of huge detectors installed at high energy physics accelerators detecting particle and photon tracks after beam collisions. In both cases, the so-called time-of-flight (TOF) techniques are used [5] where a key role is played by the timing coincidence resolution parameter that, in today's commercial PET machines, is of the order of 500 ps. Achieving the 10 ps milestone in timing coincidence resolution would allow avoiding reconstruction algorithms in data processing in TOF-PET and increasing the sensitivity by at least one order of magnitude [4,6]. For this application, it is particularly important the rise time of the luminescence signal, following the arrival of the excitation photon, as this eventually determines the limit in the coincidence time resolution. Short decay time of the luminescence is also relevant to squeeze the generated luminescence photons in a short time window. Despite the importance for applications, until now only few studies addressed the analysis of the scintillation dynamics with sub-10 ps time resolution (see for instance [7,8]). In order to gain access to luminescence rise and decay dynamics in the sub-10 ps time scale, detection schemes typically employ a streak camera.

Scintillators suitable for such a goal must show not only high light yield, but also very fast scintillation response in the time scale of several nanoseconds - few tens of nanoseconds, and with a negligible risetime [6]. The so-called free Wannier exciton emission in wide direct-gap semiconductors could offer such characteristics [9,10], but due to its inevitable small Stokes shift, it is impossible to exploit it in bulk scintillation elements as all the scintillation emission would be re-absorbed [11] These materials are usually studied in nanocrystalline powder, thin film or nano-composite forms [12]. In the latter case the aim is to provide a transparent bulk optical element with the desired scintillation characteristics which are defined by fine nanocrystallite scintillator phase, homogeneously dispersed in the volume of the host.

Further enhancement of the desirable properties of Wannier exciton

* Corresponding author at: Istituto Nazionale di Ottica - Consiglio Nazionale delle Ricerche CNR-INO Sede di Sesto Fiorentino, Via Madonna del Piano 10, Sesto Fiorentino, FI 50019, Italy.
E-mail address: guido.toci@ino.cnr.it (G. Toci).

https://doi.org/10.1016/j.jlumin.2018.12.034
Received 1 October 2018; Received in revised form 4 December 2018; Accepted 17 December 2018
Available online 18 December 2018

can be achieved due to so called quantum size effect. This effect results in an enhanced stability and accelerated decay of the exciton state when the exciton motion is confined in one, two or three dimension, in so-called quantum wells, wires and dots, respectively. One of the first examples of 1D (quantum well) confined structure featuring large light output and fast scintillation response was presented by K. Shibuya et al. [13] employing lead-halide-based perovskite-type layers made of $[PbX_4]^{2-}$ (X = Br, I), sandwiched between two insulating layers of alkylammonium, resulting in a fast decay time of 390 ps and a risetime in the scale of tens of ps, under excitation of 20 ps electron pulses.

From a practical point of view an interesting option is offered by epitaxial technologies where multiple quantum well (MQW) structures of alternating GaN and InGaN layers, each one a few nanometers thick, are prepared on Al_2O_3 substrates with the lateral dimensions up to several inches. Excitonic emission occurs in InGaN layers in the spectral range 400–450 nm and can achieve subnanosecond photoluminescence decay times [14]. Time-resolved luminescence of these MQW structures was also investigated in [15–17]. Such a nanostructure was found to be an interesting candidate for fast scintillation detector of soft X-ray or low energy particles [18]. Nonetheless, the ultimate quantitative rise time characteristics of luminescence decay in these materials have never been determined so far. In this context, we focus here on the rise time measurements and excitation density effect of a InGaN/GaN MQW scintillator, investigated by means of femtosecond laser excitation and streak camera detection. The appropriate convolution procedures in the data handling have been used to obtain their correct quantitative evaluation.

2. Sample description and preparation

Structure with InGaN/GaN MQWs (see Fig. 1) used in our experiment have been prepared by an Aixtron 3 × 2 CCS MOVPE system equipped with a Laytec EpiCurve TT apparatus for in situ measurement of reflectivity. The structure contains 6 groups of 5 InGaN QWs in the active region. The In content in $In_xGa_{1-x}N$ QWs is x = 0.07 ± 0.02, with QW thicknesses 1.4 ± 0.2 nm and GaN barrier thicknesses 5.7 ± 0.2 nm. Thickness was estimated from the simulation of X-ray diffraction data and the In concentration was estimated from SIMS results. Each group of five QWs was followed by a 25 nm thick GaN separation layer with the purpose of decreasing the strain energy in the active region and also to increase the thickness of the scintillator active region.

Trimethylgallium (TMGa) and NH_3 were used as precursors with a hydrogen carrier gas for the growth of buffer layers. Triethylgallium (TEGa), trimethylindium (TMIn), and ammonia with a nitrogen carrier gas were used for the growth of the InGaN QWs and barriers. Structures

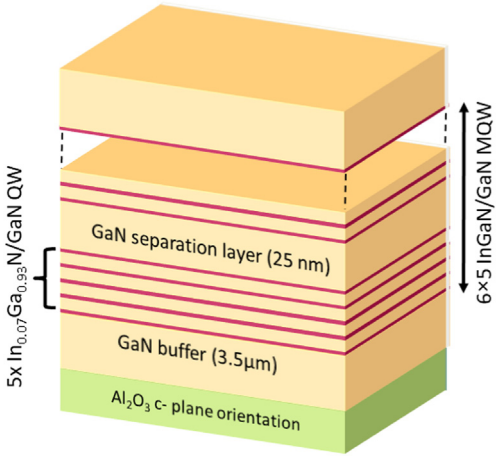

Fig. 1. Schematics of the InGaN/GaN MQW structure used in the experiments.

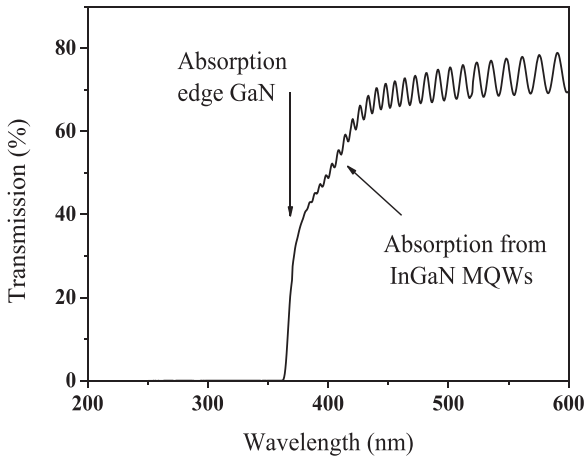

Fig. 2. Transmission spectrum at room temperature of the sample under test.

were grown on sapphire substrates with c-plane orientation. More details about the structure preparation can be found in [18].

The transmission spectrum of the sample used in the experiments is shown in Fig. 2. From this spectrum it can be seen that it is possible to excite selectively the InGaN quantum wells in the band ~ 380–420 nm, whereas an excitation below 350 nm will also affect the GaN in the barriers between the InGaN layers and in the separation layers between of the individual MQWs groups. The oscillating behavior in the transmission for wavelengths longer than 400 nm is due to etalon effects between the surfaces of the sample.

3. Experimental set-up and data processing

3.1. Experimental set-up

Experiments were carried out at the Intense Irradiation Laser Laboratory (ILIL) of the CNR-INO, in Pisa (Italy) (http://research.ino.it/Groups/ilil/it/about_it/). The sample is excited by laser pulses at about 266 nm and 400 nm obtained as the 3rd and 2nd harmonics respectively, of a Ti:Sapphire amplified laser system, delivering pulses with a duration of 80 fs at 800 nm [19]. After the conversion to the 2nd and 3rd harmonics the pulse duration is less than 200 fs for both wavelengths. The incident energy is of a few tens of μJ, with a spot size on the target of about 2 mm in radius. The experimental set-up is depicted in Fig. 3. The detection is carried out with a Hadland Imacon 500 streak camera (spectral response from 300 nm to 650 nm, peaked at about 450 nm), fitted with an image intensifier. The streak image is acquired by a cooled Electron Multiplying CCD camera (Andor LUCA, 1002 × 1004 pixels). The streak camera is triggered by a signal derived from the laser pulse; an adjustable delay box allows for the fine tuning of the trigger delay. The streak camera has various scan speeds, from 11.1 ps/mm to 356 ps/mm, corresponding to different values of time resolution and time acquisition window. The sample is illuminated by

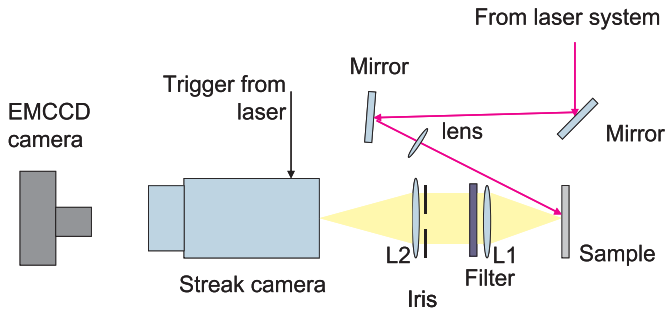

Fig. 3. Schematics of the experimental set-up (not in scale).

the laser pulse with an angle of incidence of about 16° with respect to the optical axis of the collecting optics. The sample surface is placed approximately perpendicular to the optical axis of the collecting optics, with the MQW structure facing the incident beam; the other side (Al_2O_3 substrate) is translucent. The fluorescence of the sample is imaged on the streak camera slit by the lenses L_1, L_2. matching the entrance $f/\#$ of the streak camera. The spectral band of interest is selected by a suitable filter placed between the two lenses. An iris between the two lenses is used to adjust the signal intensity reaching the streak camera.

The emission spectra of the sample were collected at the input of the streak camera using a fiber coupled spectrometer (Ocean Optics).

Careful calibration procedures are needed in all the experiments performed with streak camera systems. Attention must be paid to avoid the saturation of both the photocatode of the streak tube, and of the image intensifier, which can lead to severe distortions in the acquired signal.

The intensity response of the streak camera was calibrated to compensate spatial non-uniformities in the photocathode for the streak tube and in the intensifier luminosity. This calibration was carried out by acquiring the decay traces of fluorophores having a decay time of some hundreds of ns, which provide a signal which is temporally uniform (within few %) over a time interval of few ns. The scan speed in the different time scales was calibrated by analyzing the signals obtained from laser pulse pairs with known temporal separation, obtained by reflection on both surfaces of different glass plates with known thicknesses.

The streak traces were acquired on a shot by shot basis. After acquisition the individual traces were processed with the following steps:

- The intensity was corrected using the previously acquired intensity calibration traces, to compensate for spatial non-uniformities in the photocatode for the streak tube and in the intensifier luminosity;
- The time scale was re-sampled at uniform time intervals, using the previously acquired position vs. time calibration curves;
- The traces obtained from different shots (usually 10) were finally synchronized and co-averaged, using the rise front as time marker.

This procedure resulted in a high signal to noise ratio, still not compromising the temporal resolution of the acquisition system. Conversely, a direct averaging of multiple shots would result in a degradation of the temporal resolution of the system, due to the residual jitter between the scan trigger signal and the laser pulse.

The time resolution of the acquisition system has been determined as the FWHM of the response after the excitation with a 200 fs duration laser pulse at 400 nm, and using the same processing protocol adopted for the measurements on the samples. As the laser pulse is much shorter than the time response of the system, these measurements provide the Impulse Response Function (IRF) of the system. In particular we obtained a IRF FWHM of 81.8 ps at the lowest scan speed (356 ps/mm) and of 10.2 ps at the fastest scan speed (29.5 ps/mm). Fig. 4 shows the response of the system under excitation with the laser pulses at 400 nm at the different scan speeds, as obtained after the synchronization and co-averaging procedure described above.

The decay curves were finally approximated by a sum of exponential functions convoluted with the appropriate instrumental response using the software package SpectraSolve (Ametek).

4. Experimental results

4.1. Emission spectra

The emission spectrum of MQW sample described in Section 2, under excitation at 266 nm, is reported in Fig. 5 below. Even though the UV laser emission is cut off by the glass of the collection optics, a bandpass filter (Filter #1, Oriel 5–58, peak wavelength 430 nm, bandwidth 30 nm FWHM) was used to avoid possible spectral

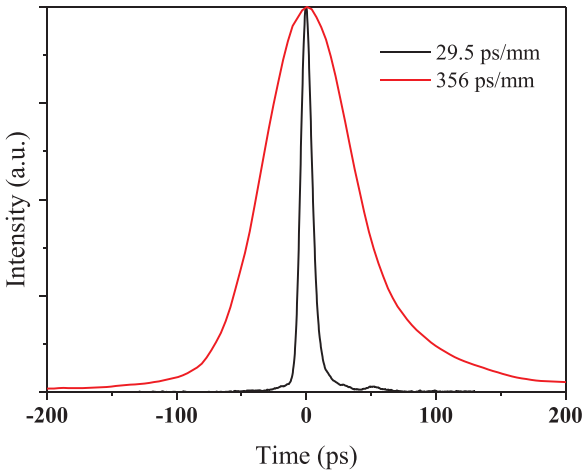

Fig. 4. IRF to the laser pulses at 400 nm at the scan speeds used in the measurements. The traces are normalized to their peak value.

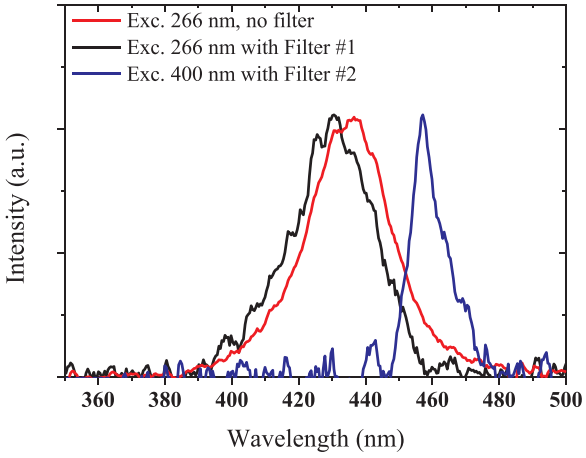

Fig. 5. Excitonic emission of the MQW quantum well structure under 266 nm (with and without the interferential Filter #1) and 400 nm excitation (after the Filter #2 used to reject the excitation radiation). All the plots were rescaled to their peak value. The Filters #1 and #2 are described in the text.

contamination on the signal (such as residual laser 2nd harmonic). A single emission band peaked at 437 nm was observed. We observe that no further band in the yellow region of the spectrum (which was reported in [18,20]) was detected.

When exciting at 400 nm a different bandpass filter (Filter #2, Andover 450FS20–50 peaked at 450 nm, bandwidth 20 nm) was used because the laser was partially superimposed to the emission band. This allowed to collect the MQW exciton emission tail at longer wavelengths.

4.2. Luminescence decay

The temporal dependence of the emission was acquired under excitation at 266 nm and 400 nm. At 266 nm two excitation conditions were used, i.e. lower incident pulse energy (16 μJ, corresponding to approximately 0.4 mJ/cm^2 of average excitation fluence) and a higher one (29 μJ, i.e. 0.7 mJ/cm^2). The emission signal was filtered using the Filter #1 (see above). Under excitation at 400 nm the decay behavior was acquired with an incident energy of 30 μJ (about 0.7 mJ/cm^2 of fluence), using the Filter #2 to select the detection spectral band.

For each excitation, the luminescence signal was acquired with two different settings of the streak camera: the fastest available scan speed, capable to achieve the highest time resolution (i.e. 10.2 ps of IRF FWHM) over a short time window (about 700 ps), and a slower scan

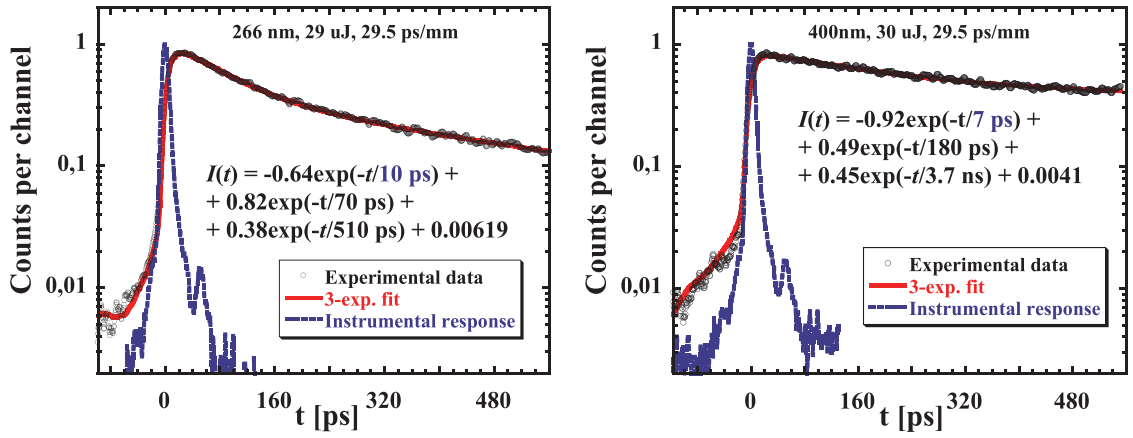

Fig. 6. Luminescence decay with high temporal resolution (nominal scan speed 29.5 ps/mm) and with the same excitation conditions as in Fig. 4. Solid line is convolution of IRF (also in figure) and function $I(t) = A_1 \times exp(-t/T_1) + A_2 \times exp(-t/T_2) + A_3 \times exp(-t/T_3) + Background$. Fitting parameters are reported in the figure. Detection under excitation at 266 nm is made with Filter #1, under excitation at 400 nm is made with Filter #2 (see Fig. 5).

speed, capable to record a relatively long time interval (about 10 nsec) with a lower time resolution (IRF 81.8 ps, see above). The fast acquisition mode was specifically aimed to determine the rise time of the luminescence response after the excitation, which is the main target of the experiment. The slow acquisition mode addressed the evaluation of the decay behavior, mainly for comparison with previous results [18].

At the fastest scan speeds the rise time could be resolved reliably in the decay curves, over a dynamic range of about 2 decades. The rising edge of the luminescence was analyzed using the fast 29.5 ps/mm scan speed (Fig. 6). The rising part of the curve was fitted by means of a negative exponential function, whose rise time is 10 ps (under excitation at 266 nm) and 7 ps (under excitation at 400 nm). IRF was convoluted with the decay function *I(t)* to obtain the fit.

The examples of resulting decays are shown in Fig. 7. Apparently, the departure from single exponential behavior is more evident in case of 266 nm excitation. We did not find any substantial difference in the decay shape for two excitation densities of 16 and 29 μJ used in the case of 266 nm excitation.

The decaying part of curve is approximated by different decay times compared with Fig. 6 due to much longer time scale and non-exponential character of the decay (see Section 5).

It must be noticed that the structure of the sample itself introduces a slowdown in the rise time of the luminescence. The MQW structure has an overall thickness of less than 4 μm, which is negligible in terms of propagation delay of the excitation and signal light. On the other hand the sample has an overall thickness of about 0.45 mm, mostly constituted by the Al_2O_3 substrate, whose back face is diffusing. The group velocity of light in Al_2O_3 at 430 nm (the peak of the emission wavelength) is $c/1.84$. The path difference between the signal generated at the front surface and travelling toward the streak camera, and the signal generated at the front surface travelling toward the back side and reflected back to the streak camera results in a time delay inside the sample of about 5.5 ps (neglecting slanted paths and multiple reflections). This figure is not negligible with respect to the measured rise time, and it is not included in the evaluation of the IRF discussed above (the latter was obtained by sending the laser beam on a surface diffuser in place of the sample, and therefore it is not affected by the optical thickness of the target).

5. Discussion and conclusions

The measurement shown above demonstrate that the luminescence of the MQW under test has a rise time of the luminescence in the sub-10 ps time scale. By using convolution procedure with the measured IRF for the fast streak camera scan (29.5 ps/mm) we have reliably resolved the presence of comparable and very small rise time values on the range 7–10 ps in the luminescence emission mechanism under both the 266 and 400 nm excitations. The former excitation involves also massive charge carrier migration from the GaN nanolayers into InGaN ones where the luminescence process occurs. The obtained results mean that this charge carrier migration does not add any delay in the photoluminescence mechanism. It must be noticed that the actual rise time

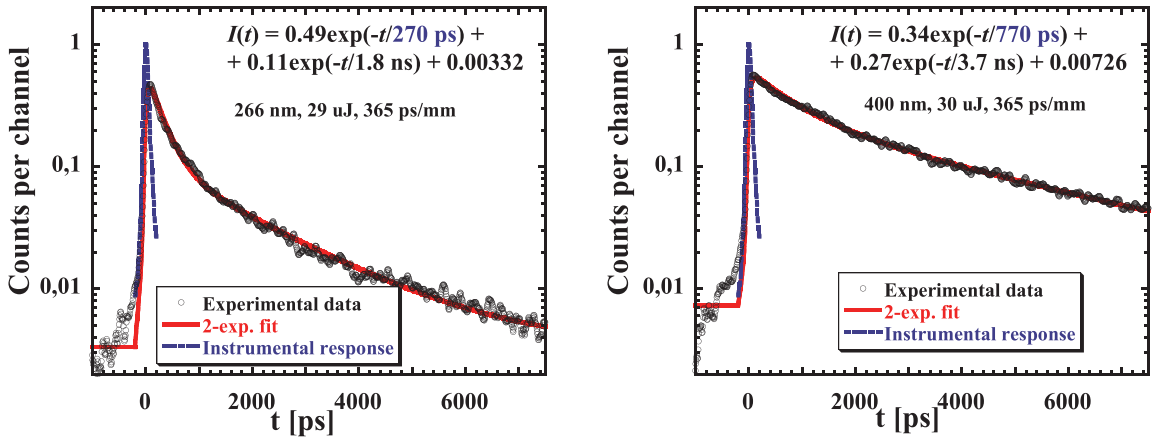

Fig. 7. Decay curves for the excitation at 266 nm (energy 29 μJ) and 400 nm (energy 30 μJ). Solid line is convolution of IRF (also in figure) and function $I(t) = A_1 \times exp(-t/T_1) + A_2 \times exp(-t/T_2) + Background$. Fitting parameters are reported in the figure. Detection under excitation at 266 nm is made with Filter #1, under excitation at 400 nm is made with Filter #2 (see Fig. 5).

could be even shorter, as the calculated rise time is comparable with the detection system IRF, and the luminescence rise time could be affected by light scattering effects at the level of 5 ps.

Regarding the decay behavior, the discrepancy in the value of the decay time resulting from the analysis shown in Figs. 6 and 7 should be understood just as resulting from technical reasons which does not necessarily reflect the physical nature of the process. In particular, the relatively low temporal resolution in the slower acquisition time scale (356 ps/mm) does not allow to obtain a reliable information on the fast component of the decay; conversely, in the fastest scan speed (29.5 ps/mm) it is possible to resolve the rise time and the fastest decay component, but the acquisition time scale is too short to obtain a reliable assessment of the slowest decay component. It must be noticed anyway that the measurement of the slow decay components (in the time scale of several ns) is routinely carried out with more conventional techniques (e.g. time correlated single photon counting [18]).

While single exponential photoluminescence decay was reported only in the case of the measurement of a single InGaN/GaN quantum dot (QD) [21], the measurement over an ensemble of QDs [22] or in MQW structure [23] always shows a non-exponential decay profile, which has been approximated e.g. by a stretched-exponential model and explained by local compositional fluctuations [23].

An interesting aspect, however, is the difference of the decay profiles under 400 nm and 266 nm excitations. Namely, the decay is noticeably accelerated in the latter case. In part, such a difference can be due to the detection of emission in somewhat different spectral parts of excitonic band due the used filters (see Section 4.2 above). However, given the peak power of the excitation laser, the excitation density effects should be also considered. In the context of non-proportionality of scintillator materials, it has been considered that various interactions between elementary closely spaced excitations and charge carriers in the conversion stage of scintillation mechanism (first few picoseconds) induce energy losses [24]. While such a process heavily affects the light yield of a scintillator, it does not show any influence on the luminescence decay itself as it occurs before the relaxed excited state of emission centers is formed. However, noticeable distortion of the decay was noted when high intensity femtosecond pulse laser source at 313 nm (Urbach tail of absorption edge of $CdWO_4$) was used for the excitation of a $CdWO_4$ single crystal scintillator [25]. Gradually increasing deviation of the decay from single exponential (acceleration of the decay) with increasing laser power was successfully modeled by the Forster dipole-dipole interaction model which works on the relaxed self-trapped exciton states of $CdWO_4$. Even if such a process has been forecasted to occur in semiconductors above much higher threshold (compared to ionic crystals as $CdWO_4$) of the onset of self-quenching due to differences in the mobility of holes, electrons and excitons [26] we tend to explain the above reported difference in the decay shape on the excitation wavelength in the same way: in case of 266 nm excitation the band-to-band absorption transition of GaN is involved and the total absorption coefficient of MQW will be much higher compared to that at 400 nm when only InGaN nanolayers are absorbing, as it was pointed out in Section 2. Thus, total deposited energy in MQW structure will be much higher as well in case of 266 nm excitation. However, all generated electrons and holes in MQW tend to migrate into the InGaN nanolayers which create the lowest-energy band structure for both electrons and holes. In spite of possible migration losses, the density of excitonic states in these regions will be much higher for 266 nm excitation and, consequently, their interaction probability strongly increases. Such interaction of excitons is completely analogous to the above mentioned situation in $CdWO_4$ and it shows itself qualitatively exactly in the same way. We also note that simple increase of excitation density by factor less than two in case of 266 nm excitation did not show any clear difference in the decay course.

In conclusion, our measurements have demonstrated that InGaN/GaN heterostructures feature a luminescence response with rise time of less than 10 ps; this value can still be lengthened by instrumental and experimental effects, so that it must be considered as an upper limit of the actual rise time. The timing characteristics of MQW are thus not deteriorated due to rising edge of the luminescence response, which is of great importance for its use in superfast scintillation detectors. Moreover, luminescence decay and in particular the luminescence rise time did not show an appreciable dependence on the excitation density, which is also an important feature in view of practical applications.

Acknowledgments

Financial support of Czech National Foundation grant no. 16-15569S and European project COST, FAST TD1401 are gratefully acknowledged. We also acknowledge funding from the CNR funded Italian research Network ELI-Italy (D.M. n. 631 08.08.2016).

References

[1] M. Nikl, A. Yoshikawa, Recent R&D trends in inorganic single crystal scintillator materials for radiation detection, Adv. Opt. Mater. 3 (2015) 463–481.
[2] P. Lecoq, Development of new scintillators for medical applications, Nucl. Instrum. Methods Phys. Res. A809 (2016) 130–139.
[3] M. Conti, Focus on time-of-flight PET: the benefits of improved time resolution, Eur. J. Nucl. Med. Mol. Imaging 38 (2011) 1147–1157.
[4] T. Jones, D. Townsend, History and future technical innovation in positron emission tomography, J. Med. Imag. 4 (2017) 011013.
[5] S. Gundacker, F. Acerbi, E. Auffray, A. Ferri, A. Gola, M.V. Nemallapudi, G. Paternoster, C. Piemonte, P. Lecoq, State of the art timing in TOF-PET detectors with LuAG, GAGG and L(Y)SO scintillators of various sizes coupled to FBK-SiPMs, J. Instrum. 11 (2016) P08008.
[6] P. Lecoq, Pushing the limits in time-of-flight PET imaging, IEEE Trans. Radiat. Plasma Med. Sci. 1 (2017) 473–485.
[7] T. Shimizu, K. Yamanoi, K. Sakai, M. Cadatal-Raduban, T. Nakazato, N. Sarukura, M. Kano, A. Wakamiya, D. Ehrentraut, T. Fukuda, M. Nagasono, T. Togashi, S. Matsubara, K. Tono, A. Higashiya, M. Yabashi, H. Kimura, H. Ohashi, T. Ishikawa, Response time-shortened zinc oxide scintillator for accurate single-shot synchronization of extreme ultraviolet free-electron laser and short-pulse laser, Appl. Phys. Express 4 (2011) 062701.
[8] H. Burešová, L. Procházková, R.M. Turtos, V. Jarý, E. Mihóková, A. Beitlerová, R. Pjatkan, S. Gundacker, E. Auffray, P. Lecoq, M. Nikl, V. Čuba, Preparation and luminescence properties of ZnO:Ga – polystyrene composite scintillator, Opt. Express 24 (2016) 15289–15298.
[9] S.E. Derenzo, M. Weber, M.K. Klintenberg, Temperature dependence of the fast, near-band-edge scintillation from CuI, HgI_2, PbI_2, ZnO:Ga and CdS:In, Nucl. Instr. Meth. Phys. Res. A 486 (2002) 214–219.
[10] E.D. Bourret-Courchesne, S.E. Derenzo, M.J. Weber, Development of ZnO:Ga as an ultra-fast scintillator, Nucl. Instr. Methods. Phys. Res. A 601 (2009) 358–363.
[11] D. Ehrentraut, H. Sato, Y. Kagamitani, A. Yoshikawa, T. Fukuda, J. Pejchal, K. Polak, M. Nikl, H. Odaka, K. Hatanaka, H. Fukumura, Fabrication and luminescence properties of single-crystalline, homoepitaxial zinc oxide films doped with tri- and tetravalent cations prepared by liquid phase epitaxy, J. Mater. Chem. 16 (2006) 3369–3374.
[12] E.A. McKigney, R.E. Del Sesto, L.G. Jacobsohn, P.A. Santi, R.E. Muenchausen, K.C. Ott, T.M. McCleskey, B.L. Bennett, J.F. Smith, D.W. Cooke, Nanocomposite scintillators for radiation detection and nuclear spectroscopy, Nucl. Instr. Methods. Phys. Res. A 579 (2007) 15–18.
[13] K. Shibuya, M. Koshimizu, H. Murakami, Y. Muroya, Y. Katsumura, K. Asai, Development of ultra-fast semiconducting scintillators using quantum confinement effect, Jpn. J. Appl. Phys. 43 (2004) L1333–L1336.
[14] T.S. Ko, T.C. Lu, T.C. Wang, J.R. Chen, R.C. Gao, M.H. Lo, H.C. Kuo, S.C. Wang, J.L. Shen, Optical study of -plane InGaN/GaN multiple quantum wells with different well widths grown by metal-organic chemical vapor deposition, J. Appl. Phys. 104 (2008) 093106.
[15] S. Miasojedovas, S. Juršėnas, G. Kurilčik, A. Žukauskas, V. Ivanov, M. Godlewski, M. Leszczyński, P. Perlin, T. Suski, Luminescence in highly excited InGaN/GaN multiple quantum wells grown on GaN and sapphire substrates, Acta Phys. Pol. A 106 (2004) 273–279.
[16] A.N. Cartwright, M.C.-K. Cheung, F. Shahedipour-Sandvik, J.R. Grandusky, M. Jamil, V. Jindal, S.B. Schujman, L.J. Schowalter, C. Wetzel, P. Li, T. Detchprohm, J.S. Nelson, Ultrafast carrier dynamics and recombination in green emitting InGaN MQW LED, Mater. Res Soc. Symp. Proc. 916 (2006) (0916-DDO4-10).
[17] A. Jaros, J. Hartmann, H. Zhou, B. Szafranski, M. Strassburg, A. Avramescu, A. Waag, T. Voss, Photoluminescence of planar and 3D InGaN/GaN LED structures excited with femtosecond laser pulses close to the damage threshold, Sci. Rep. 8 (2018) 11560.
[18] A. Hospodková, M. Nikl, O. Pacherová, J. Oswald, P. Brůža, D. Pánek, B. Foltynski, E. Hulicius, A. Beitlerová, M. Heuken, InGaN/GaN multiple quantum well for fast scintillation application: radioluminescence and photoluminescence study, Nanotechnology 25 (2014) 455501.
[19] L.A. Gizzi, C. Benedetti, C.A. Cecchetti, G. Di Pirro, G. Gamucci, G. Gatti, A. Giulietti, D. Giulietti, P. Koester, L. Labate, T. Levato, N. Pathak, F. Piastra, Laser-

plasma acceleration with FLAME and ILIL ultraintense lasers, Appl. Sci. 2013 (3) (2013) 559.
[20] A. Hospodková, J. Oswald, M. Zíková, J. Pangrác, K. Kuldová, K. Blažek, G. Ledoux, C. Dujardin, M. Nikl, On the correlations between the excitonic luminescence efficiency and the QW numbers in multiple InGaN/GaN QW structure, J. Appl. Phys. 121 (2017) 214505.
[21] M. Winkelnkemper, M. Dworzak, T.P. Bartel, A. Strittmatter, A. Hoffmann, D. Bimberg, Origin of the broad lifetime distribution of localized excitons in InGaN/GaN quantum dots, Phys. Stat. Sol. (b) 245 (2008) 2766–2770.
[22] S.F. Chichibu, T. Onuma, T. Aoyama, K. Nakajima, P. Ahmet, T. Chikyow, T. Sota, S. DenBaars, Nakamura, T. Kitamura, Y. Ishida, H. Okumura, Recombination dynamics of localized excitons in cubic In x Ga 1 − x N/GaN multiple quantum wells grown by radio frequency molecular beam epitaxy on 3C–SiC substrate, J. Vac. Sci. Technol. B 21 (2003) 1856–1996.
[23] S. Khatsevich, D.H. Rich, X. Zhang, P.D. Dapkus, Correlating exciton localization with compositional fluctuations in quantum wells grown on GaN planar surfaces and facets of GaN triangular prisms, J. Appl. Phys. 102 (2007) 093502.
[24] G. Bizarri, W.W. Moses, J. Singh, A.N. Vasil'ev, R.T. Williams, An analytical model of nonproportional scintillator light yield in terms of recombination rates, J. Appl. Phys. 105 (2009) 044507.
[25] S. Markov, V. Nagirnyi, A. Vasil'ev, V. Makhov, R. Laasner, S. Vielhauer, M. Kirm, R. Grigonis, V. Sirutkaitis, Modelling of decay kinetics of self-trapped exciton luminescence in $CdWO_4$ under femtosecond laser excitation in absorption saturation conditions, Cent. Eur. J. Phys. 10 (2012) 1002–1008.
[26] W.W. Moses, G.A. Bizarri, R.T. Williams, S.A. Payne, A.N. Vasil'ev, J. Singh, Q. Li, J.Q. Grim, W.-S. Choong, The Origins of Scintillator Non-Proportionality, IEEE Trans. Nucl. Sci. 59 (2012) 2038–2044.